Journal of Applied Electrochemistry **34**: 277–281, 2004.

On the observation of inductive high-frequency impedance behaviour during the electrodeposition of Au–Sn alloys

BENEDETTO BOZZINI[1,*], CLAUDIO MELE[1] and IVONNE SGURA[2]
[1]*Dipartimento di Ingegneria dell'Innovazione, Università di Lecce, v. Monteroni, I-73100 Lecce, Italy*
[2]*Dipartimento di Matematica, Università di Lecce, v. Monteroni, I-73100 Lecce, Italy*
*(*author for correspondence, fax: +39-0832-325004, e-mail: benedetto.bozzini@unile.it)*

Received 29 April 2003; accepted in revised form 30 September 2003

Key words: Au alloys, Au–Sn, electrochemical impedance, electrocrystallisation, electrodeposition of alloys, nucleation

Abstract

Inductive high-frequency impedance behaviour is often observed in metal electrodeposition systems. This behaviour is typically attributed to equipment limitations or non-idealities in the cell set-up and electrical connections. Such instrumental artefacts would nevertheless be relevant to a frequency range which is expected to be well above that in which inductive behaviour is in fact observed (down to a few tens of Hz). In this paper some results on an acidic Au–Sn electrodeposition system are reported. Electrochemical impedance and potentiostatic transients were measured. These results suggest that the high-frequency inductive behaviour may be related to metal nucleation processes. A correlation is proposed between the pseudo-inductive potentiostatic nucleation transients and the pseudo-inductive behaviour of the impedance spectra.

1. Introduction

It is well-known that high-frequency AC electrochemical impedance (henceforward EI) measurements often exhibit inductive behaviour. This phenomenon is commonly attributed to equipment artefacts [1, 2]. This attribution is often correct, but it may not necessarily be general. We feel that some electrocrystallisation processes may be an exception. In EI data reported in the metal electrodeposition literature the highest frequency shown is often in the kHz range or lower. One can assume that experimental points measured at higher frequencies exhibit inductive behaviour. In some instances a few high-frequency inductive experimental points preceding the capacitive ones appear in published EI spectra (e.g. [3, 4]). To the best of the authors' knowledge, the highest starting frequencies are reported for Zn electrodeposition from alkaline (11–50 kHz [5]) and acidic solutions (12–100 kHz [6], 10–100 kHz [7], 60–100 kHz [4]). Nevertheless, data for acidic sulphate zinc electrodeposition baths in the presence of Pb^{2+} were reported to start from frequencies as low as 100 Hz [8]. Visual inspection of the EI loci published in these papers discloses that the starting frequency is a potential-dependent quantity. Lower starting frequencies correlate with higher cathodic polarisation. This fact seems to hint at electrochemical, rather than instrumental effects, even if the dynamic behaviour of the circuitry may still have a bearing, as discussed below.

Recently some accurate methodological work on EI measurements for electrodeposition applications was published, e.g. [4, 6, 9–11]. Nevertheless we were unable to find any references dealing in a systematic way with the peculiarities of the high-frequency behaviour in similar systems. Inductive elements were reported in the equivalent-circuit representations of electrodeposition systems e.g. [12], but not in a configuration leading to high-frequency effects. Some peculiarities of the EI inductive behaviour in the low-frequency range, related to the growth of real crystal faces, were reported [13].

In this work we examine results concerning the electrodeposition of Au–Sn alloys. This system has been studied previously by our group, stressing the electrochemical behaviour [14, 15] and the compositional and crystallographic nature of the deposits [16].

2. Experimental

2.1. *Impedance measurements*

2.1.1. *Cell, electrodes and electrolytes*

A specially designed cylindrical coaxial plexiglas cell was employed. The cell was designed according to the recommendations of [12]. In order to shield the cell from external disturbances the cylinder was lined with a grounded stainless steel grid. The working electrode was a disc embedded in an axially mounted cylindrical PTFE

holder. A glassy carbon electrode (AMEL 492/GC3) was employed, whose immersion potential in the electrodeposition solution was stable at 510 ± 4 mV vs Ag/AgCl. The counter electrode was a large-area wound Pt wire ring giving rise to a uniform current density distribution and minimising the cell gain. This electrode set-up ensures a good approximation of a plane-parallel electrode configuration, whose advantages for EI measurements were proven.

In order to minimise the phase shift at high-frequencies caused by high-resistance standard reference electrodes, a capacitively coupled Pt wire was used as a pseudo-reference electrode [17]. The potentials are reported on the Ag/AgCl scale for ease of reference. The stability of the potential measured with the pseudo-reference electrode vs an Ag/AgCl electrode in the relevant electrolyte was found to be largely satisfactory: after a stabilisation period of less than 5 min., the only disturbances are long-term fluctuations with spectral components lower than 2 MHz. The reference electrode wire tip was formed in the shape of a hook; the wire connection was embedded into a cylindrical PVC holder fixed along the axis of the cell. The reference electrode was located in front of the working electrode at a distance of *ca.* 1 mm. The high conductivity of the electrolyte employed ensured minimal gap effects on the impedance behaviour [1].

The electrodeposition bath contained Au 5 g l^{-1} (as $KAu(CN)_4$) and Sn 75 g l^{-1} (as $SnCl_4 \cdot 5H_2O$) and was acidified to pH 0.5 with HCl. The calibration Zn bath was an HCl solution at pH 0.5 containing 1 M $ZnCl_2$.

2.1.2. *Cell impedance*

Accurate evaluation of electrode impedance can be affected by the counter-electrode dynamics. In fact the working electrode current response depends on the cell impedance. Assuming that: (i) the potentiostat gain is real, (ii) the electrical response of the whole cell as well as that of the working- and counter-electrodes are linear and (iii) the counter-electrode behaves like the parallel of a Faradaic impedance and a double-layer capacitance, the distortion of the working-electrode impedance introduced by the counter-electrode impedance displays a maximum as their Faradaic impedances and double-layer capacities separately change from zero to infinity. The only *a priori* approach to the minimisation of this distortion is the separate minimisation of the Faradaic resistance and of the double layer capacity of the counter-electrode. A large-area counter-electrode and a uniform current-density distribution are adequate cell-design solutions for this purpose.

2.2. *Electric equipment*

EI spectroscopy (henceforward EIS) measurements were performed using a Frequency Response Analyser (Solartron SI 1250) connected to an AMEL 5000 potentiostat. The potential modulation amplitude was 10 mV.

2.2.1. *High-frequency instrumental problems and requirements*

The electronic basis of instrumental frequency limitations is the gain-dependent roll-off frequency of the operational amplifiers used in the potentiostat. A practically more stringent limitation is posed by the actual potentiostat gain, since the superior frequency limit is downscaled about linearly by the gain G [18]. Therefore the actual frequency limitation ω_L for a given experiment (assuming steady-state conditions) can be expressed as: $\omega_L = \omega_M/G$. The potentiostat gain is given by the ratio of the working-counter and working-reference voltage differences. In order to keep the gain as close as possible to 1, it is advisable to use the same material for the reference and the counter-electrode (in this case Pt) and a large counter-electrode. We measured the potentiostat gain by recording the working-counter potential difference and ratioing it to the imposed working-reference voltage. This is, of course, a potential-dependent quantity, typically ranging in the interval 1–2.5 in the present investigation. If ω_L is known, impedance data can be corrected [2]. This correction method was employed in this investigation, even though its quantitative effects are limited, owing to the low gain values and limited gain variations exhibited by our setup.

Effects of cabling parasitic inductances, which can be critical for low impedances, are expected in the 100 kHz range. Screened leads of different lengths were used and calibration experiments were run with suitable RC circuits. An optimal connection set-up was identified allowing accurate capacitive spectra to be recorded at frequencies as high as 50 kHz, the operating upper limit of the equipment being 65 kHz. The stray inductive behaviour due to current measuring resistors is also accounted for with this calibration procedure.

2.2.2. *Electrochemical calibration*

The behaviour of this set-up was checked against a well-known electrodeposition system. An acidic Zn electrodeposition bath was employed of composition similar to that of the Au–Sn bath. The spectra reported in Figure 1 shows raw data, uncorrected for gain. The imaginary part of the EI vanishes at $\omega_o = 29230$ Hz for −0.9 V and at 18440 Hz for −1.0 V. Inductive behaviour is observed at frequencies higher than ω_o. EI loci measured at frequencies lower than ω_o can be straightforwardly interpreted according to the literature on Zn electrodeposition from acidic chloride solutions.

2.2.3. *Data acquisition*

Two signal integration cycles were used in order to minimise the effects of frequency-change transients possibly introduced by the FRA and to improve the signal stability in the low-frequency range. No appreciable changes in the high-frequency portion of the EIS spectra were noticed by changing the integration cycle in the range 0.2–2 cycles.

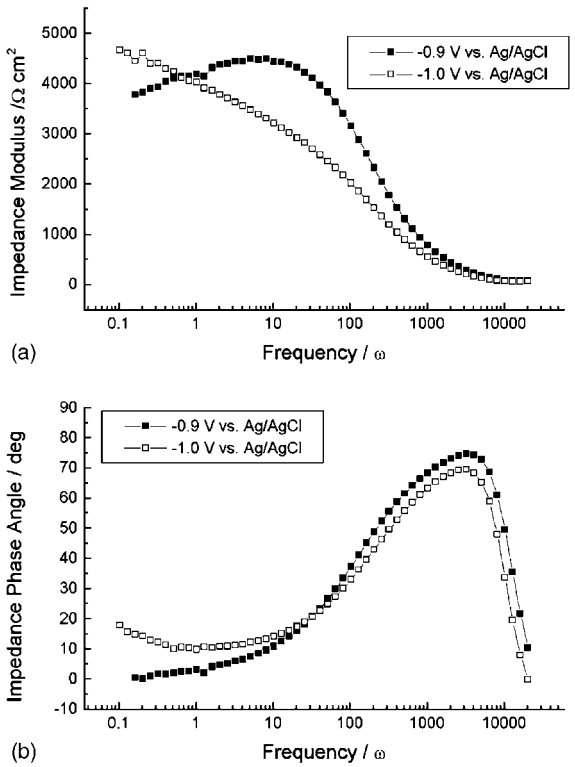

Fig. 1. Impedance spectra for the acidic chloride Zn bath. Spectra measured at −0.9 and −1.0 V vs Ag/AgCl.

3. Results and discussion

3.1. *Potentiostatic transients*

Potentiostatic current density transients were measured with potentials in the range −600 to −1300 mV in order to study the nucleation behaviour on GC electrodes (Figure 2). The potentials are reported on the Ag/AgCl scale because the overvoltage is an ill-defined quantity in this system. It depends on the alloy composition and structure, which change with applied potential and time. In addition, the immersion potential of the alloy in the plating bath is actually a corrosion potential. The rising portion of the transients is in qualitative agreement with the instantaneous nucleation model. The presence of Sn

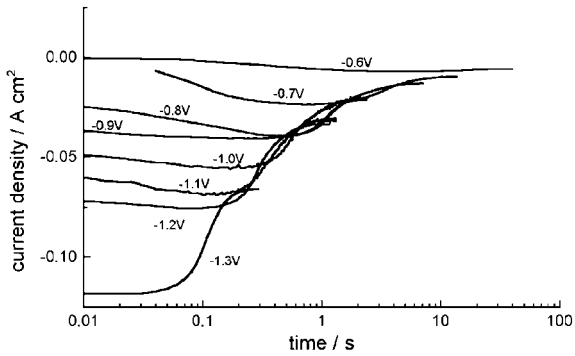

Fig. 2. Potentiostatic transients for the acidic chloride Au–Sn baths. The applied potentials are reported vs Ag/AgCl in the figure.

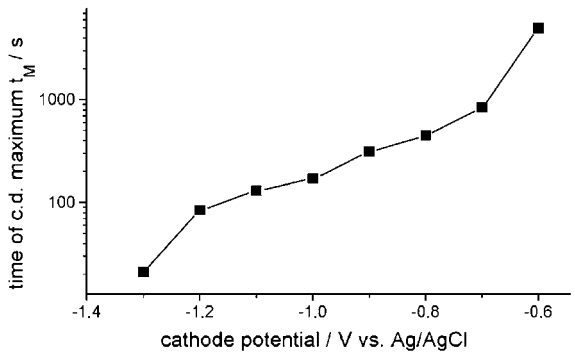

Fig. 3. Time for the maximum of the potentiostatic transients t_M as a function of the applied potential. Acidic chloride Au–Sn bath.

stabilises instantaneous nucleation even at low cathodic potentials owing to its normal electrokinetic behaviour [19].

The time to the maximum of a transient t_M can be related to the saturation nuclei density N_S (cm^{-2}): $t_M \sim N_S^{-1/2}$ [20]. Figure 3 shows that t_M varies with the cathodic potential in a roughly exponential way, indicating an increasing number of growing centres.

3.2. *EIS measurements*

The potentiostatic alloy electrodeposition EI loci (Figure 4) approximately correspond to a Randles-type

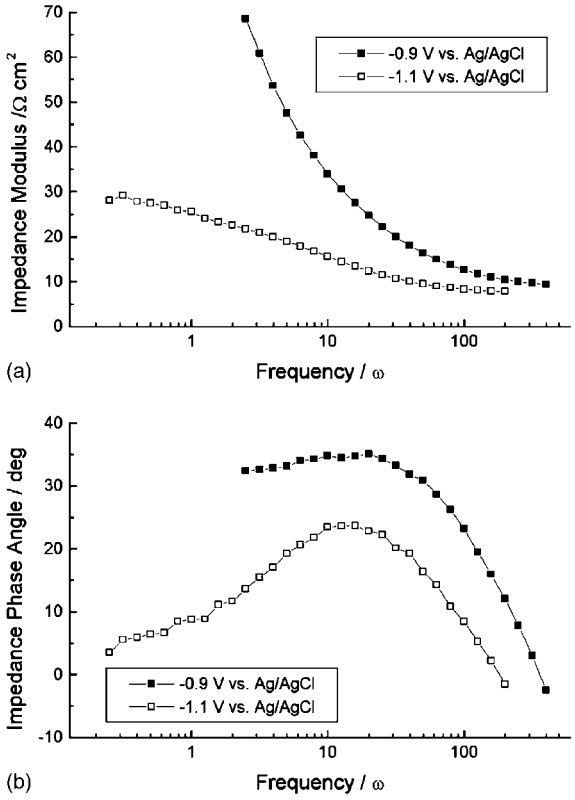

Fig. 4. Impedance spectra for the acidic chloride Au–Sn bath. Spectra measured at −0.9 and −1.1 V vs Ag/AgCl.

behaviour. Non-stationarity may be anticipated in this system, which would not anyway affect our results, which are essentially based on the sign of the phase angle. The mass-transport contribution diminishes as the cathodic polarisation increases. This can be related to the enhanced cathodic passivating activity of the cyanide released from the Au cyanocomplex at more positive potentials, where activation by Sn codeposition is less effective. The different ohmic resistance values can be related to the increase in the degree of coverage with highly conductive Au-alloy nuclei as the potential is increased in the cathodic direction.

As recalled in the Introduction, literature data on electrocrystallisation processes implicitly show that ω_o is a function of the cathodic potential. In principle, this may be an instrumental effect: higher current densities are associated with higher cathodic potentials and consequently higher potentiostat gains, depending on the specific equipment adopted and cell design. To our knowledge no gain data were reported along with electrochemical results during electrodeposition experiments. Our experimental spectra were corrected for gain effects, giving rise to hardly noticeable corrections. ω_o values were measured as a function of cathodic potential. Three independent series of data were measured (Figure 5). A highly reproducible positive correlation between cathodic potential and ω_o is observed. This correlation cannot be explained on the basis of gain effects and we can conclude that this is an electrodic effect.

3.3. *Correlation of nucleation and inductive high-frequency behaviour*

Typical potentiostatic nucleation transients ([20] and Figure 2) exhibit a time behaviour characterised by an overshoot followed by an asymptotic decay. The physical reasons for this dynamic behaviour and relevant models are the object of many reviews, e.g. [20]. This time evolution can be described as inductive, according to elementary RCL circuit theory. In the present case the transients can be explained on the basis of instantaneous nucleation. It should be noted that the theory of nucleation transients has been mainly developed for metals rather than alloys. Some pioneering work is available on alloys, the qualitative conclusions being basically the same as for the nucleation of metals [21, 22]. The present discussion is not affected by the minor differences between metal and alloy nucleation behaviour.

A value of the inductance L can be derived from the potentiostatic transients by comparing them with the time evolution of a series RCL circuit subjected to a potential step. This is a crude approximation, nevertheless the qualitative dynamic behaviour is acceptably close to that of the electrochemical system in the high-frequency limit. It can be shown that the time t_M of the first maximum for an under-damped case (displaying an overshoot) is approximately proportional to the inverse of the circuit inductance L: $t_M \sim 1/L$.

From electrochemical nucleation theory e.g. [20] it can be concluded that, in the case of instantaneous nucleation, the position in time of the current density maximum t_{MN} is related to the saturation nuclei density N_S as $t_{MN} \sim (N_S)^{-1/2}$. By identifying t_M with t_{MN}, the inductance L can be related to the saturation nuclei density N_S : $L \sim N_S^{1/2}$.

For a series RCL circuit, the high-frequency behaviour is inductive and the low-frequency one capacitive. The frequency at which the imaginary part of the EI is zero is: $\omega_o = (LC)^{-1/2}$. This quantity can thus be related to the maximum of the potentiostatic transient as: $\omega_o \sim \sqrt{t_{MN}}$. This correlation predicts the quantity $\omega_o \cdot \sqrt{t_{MN}}$ to be constant. The data shown in Figure 6 are in fair agreement with this prediction (relative standard deviation of 0.37).

It is worth observing that Zn, being a normal metal, displays a very low nuclei density. Correspondingly, macrocrystalline deposits tend to be obtained from pure metal electrolytes, unless suitable additives are used. This is probably the reason why high-frequency capacitive loops are commonly reported for Zn plating. If

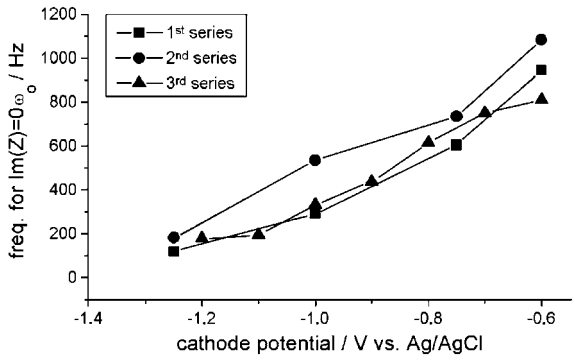

Fig. 5. Frequency at which the impedance plot crosses the imaginary axis ω_o as a function of the applied potential. Acidic chloride Au–Sn bath. Results corresponding to three independent sets of experiments are shown.

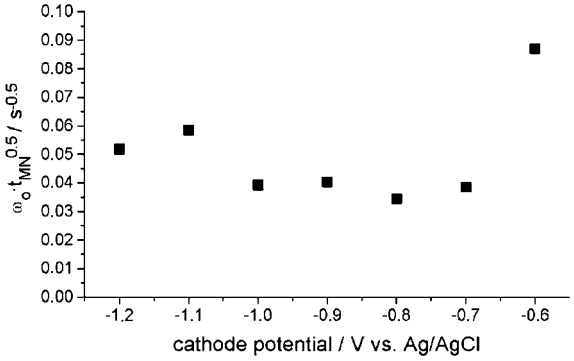

Fig. 6. The quantity $\omega_o \cdot \sqrt{t_{MN}}$ plotted as a function of the applied potential. This quantity is predicted to be constant by the nucleation model for high-frequency inductive behaviour (see Section 3.3 for details).

grain refiners are added, low values of the capacitive-loop start (100 Hz) are found [8].

4. Conclusions

Our results suggest that the high-frequency inductive behaviour of this peculiar electrodeposition system is related to metal nucleation processes. A correlation was proposed between the pseudo-inductive nucleation potentiostatic transients and the pseudo-inductive behaviour of the impedance spectra. A counter example was provided with electrodeposition from a system displaying an extremely limited nucleation behaviour and the expected frequency behaviour was found to hold experimentally.

This result may provide some guidelines to the appreciation of the bearing of equipment limitation on particular electrochemical impedance measurements. Lack of relevant insight may lead to the omission of meaningful electrochemical information. Specific non-traditional modelling, beyond the steady-state kinetics and equivalent circuit approaches, may be required to quantitatively account for the corresponding phenomena.

Acknowledgements

The authors are indebted to Ing. Paolo Lupotto (AMEL S.r.l., Milano, Italy) for building the coaxial cell and for expert advice, technical assistance and revision of the electronic aspects of this paper. Mr. Francesco Bogani's (Dipartimento di Ingegneria dell'Innovazione, Università di Lecce, Italy) continuous and qualified assistance during the EIS experiments is gratefully acknowledged.

References

1. A. Lasia, *Mod. Aspect. Electrochem.* **32** (1999) 143.
2. J. Ross Macdonald, 'Impedance Spectroscopy' (J. Wiley & Sons, N.Y. 1987), p. 213.
3. M. Holm and T.J. O'Keefe, *J. Appl. Electrochem.* **30** (2000) 1125.
4. F. Ganne, C. Cachet, G. Maurin, R. Wiart, E. Chauveau and J. Petitjean. *J. Appl. Electrochem.* **30** (2000) 665.
5. I. Epelboin, M. Ksouri and R. Wiart, *J. Electrochem. Soc.* **122** (1975) 1206.
6. D.S. Baik and D.J. Fray, *J. Appl. Electrochem.* **31** (2001) 1141.
7. C. Cachet and R. Wiart, *Electrochim. Acta* **44** (1999) 4743.
8. R. Ichino, C. Cachet and R. Wiart, *Electrochim. Acta* **41** (1996) 1031.
9. L. Pauwels, W. Simons, A. Hubin, J. Schoukens and R. Pintelon, *Electrochim. Acta* **47** (2002) 2135.
10. S. Vandeputte, E. Verboom, A. Hubin and J. Vereecken, *J. Electroanal. Chem.* **397** (1995) 249.
11. S. Goldbach, R. de Kermadec and F. Lapicque, *J. Appl. Electrochem.* **30** (2000) 277.
12. D.D. Macdonald and M.C.H. McKubre, *Mod. Aspect. Electrochem.* **14** (1982) 80.
13. E. Budevski, G. Staikov and W.J. Lorenz, 'Electrochemical Phase Formation and Growth' (VCH Weinheim (D), 1996) p. 257.
14. B. Bozzini, A. Fanigliulo, G. Giovannelli, S. Natali and C. Mele, *J. Appl. Electrochem.* in press.
15. A. Fanigliulo, P.L. Cavallotti, G. Giovannelli, C. Mele, S. Natali and B. Bozzini, *J. Solid State Electrochem.* in press
16. B. Bozzini, G. Giovannelli, S. Natali, M. Serra and A. Fanigliulo, *J. Appl. Electrochem.* **32** (2002) 165.
17. F. Mansfeld, S. Lin, Y.C. Chen and H. Shih, *J. Electrochem. Soc.* **35** (1988) 906.
18. P.R. Gray and R.G. Meyer, 'Analysis and Design of Analog Integrated Circuits' (J. Wiley Sons, N.Y, 1984) pp. 452.
19. P.L. Cavallotti, B. Bozzini, L. Nobili and G. Zangari, *Electrochim. Acta* **39** (1994) 1123.
20. T. Vargas and R. Varma, *in* R. Sarma and J.R. Selman (Eds), 'Techniques for Characterisation of Electrodes and Electrochemical Processes' (John Wiley & Sons, N.Y, 1991) p. 717.
21. P.P. Prosini, M.L. Addonizio and A. Antonaia, *Thin Solid Films* **298** (1997) 191.
22. A. Afshar, A.G. Dolati and M. Ghorbani, *Mater. Chem. Phys.* **77** (2002) 352.